Check for updates

Structure, optical simulation and thermal stability of the HfB$_2$-based high-temperature solar selective absorbing coatings

Xiao-Li Qiu,[ab] Xiang-Hu Gao,[*a] Cheng-Yu He,[a] Bao-Hui Chen[c] and Gang Liu [iD] [*ab]

Transition metal borides are a kind of potential materials for high-temperature solar thermal applications. In this work, a novel SS/HfB$_2$/Al$_2$O$_3$ tandem absorber was prepared, which exhibited high solar spectrum selectivity (α/ε) of 0.920/0.109. The optical constants of the coating were obtained using spectroscopic ellipsometry, and the dispersion model of the HfB$_2$ layer was modeled with the Tauc–Lorentz dispersion formula. In addition, the reflectance spectrum simulated by the CODE software corroborated well with the experimental results. The thermal stability test indicated that the HfB$_2$/Al$_2$O$_3$ solar absorber coating was thermally stable in vacuum at 600 °C for 2 h. When extending the annealing time to 100 h, the coating could maintain high spectral selectivity after aging at 500 °C irrespective of whether in air or vacuum. All these results indicate that the coating has good solar selectivity and is a promising candidate for high-temperature solar thermal applications.

1. Introduction

Solar energy resources are quite affluent. The radiant energy received by the earth's surface from the sun is as much as 90 000 TW, which is equivalent to burning 5.0×10^6 tons of coal. Collecting and storing solar energy have become urgent in the global effort in the reinforcement of environmentally sustainable development.[1,2] In the solar energy photothermal conversion field, the solar spectral selective absorbing coatings (SSACs) are the key devices of the solar collector. A high-quality SSAC is necessary to improve the efficiency of solar energy photothermal conversion. The SSAC is essentially an optical film, which requires high absorptance and low emittance.[3,4] The absorption mechanism of SSAC strongly depends on the macroscopic and microscopic physical properties for a solid thin film. Optical constants (refractive index n and extinction coefficient k) are essentially important parameters to understand the optical properties of the materials. For example, the extinction coefficient, k, represents the absorption of a material, and a low extinction coefficient indicates low absorption.[5]

Hafnium diboride (HfB$_2$) is a kind of transition metal boride, which has a high melting temperature, high heat resistance,

and electrical conductivity.[6,7] Most importantly, HfB$_2$ has also been proven to have intrinsic spectral selectivity because the density of free electrons in the d band of the Hf element in HfB$_2$ can be controlled to affect the optical properties.[8–10] Due to these unique capabilities, HfB$_2$ is a candidate for high-temperature SSAC applications. A small number of reports focus on the HfB$_2$ material for solar receivers in a solar tower plant. Diletta Sciti *et al.* prepared bulk HfB$_2$ for novel sunlight absorbers in solar tower plant, which exhibited the value of α/ε = 2.5 at $T = 1400$ K.[11] E. Sani *et al.* reported that the emittance for bulk HfB$_2$ was around 0.4 at temperatures between 1300 and 1450 K. When the thermal temperature increased to 1636 K, the maximum measured emittance value of HfB$_2$ was as low as 0.47.[12,13] They also confirmed that the content of secondary phases affected either the mechanical performance or the optical behavior of HfB$_2$.[14] Recently, Clara Musa *et al.* prepared SiC–HfB$_2$ (HBS) and HfB$_2$–HfC–SiC (HBCS) by the reactive spark plasma sintering technique (R-SPS). They found that the addition of SiC to HfB$_2$ (HBS) could increase solar absorbance slightly, and the value of α/ε (2.75) for HBCS surpassed that of pure boride.[9] Despite these advances in HfB$_2$, its structure, thermal stability, and optical properties are, to the best of our knowledge, totally unexplored as far as the HfB$_2$ film for the present high-temperature SSAC applications is concerned.

Here, we reported novel SS/HfB$_2$/Al$_2$O$_3$ SSAC. This tandem absorber coating essentially consisted of an absorber layer (HfB$_2$) and an anti-reflective layer (Al$_2$O$_3$). First, the structural, chemical and optical properties of the coating were studied. Second, the optical simulation was successfully investigated by phase modulated spectroscopic ellipsometry (SE) and a CODE

ᵃResearch and Development Center for Eco-Chemistry and Eco-Materials, State Key Laboratory of Solid Lubrication, Lanzhou Institute of Chemical Physics, Chinese Academy of Sciences, Lanzhou 730000, China. E-mail: gangliu@licp.cas.cn; gaoxh@licp.cas.cn

ᵇCenter of Materials Science and Optoelectronics Engineering, University of Chinese Academy of Sciences, Beijing 100049, China

ᶜState Key Laboratory of Disaster Prevention & Reduction for Power Grid Transmission and Distribution Equipment, Changsha 410007, China

commercial optical simulation software. Finally, the details of the thermal stability in vacuum and air were discussed.

2. Experimental details

A magnetron sputtering system (Kurt J. Lesker, USA) was used to deposit the HfB_2/Al_2O_3 coatings. The polished stainless steel (SS, model 316) was used as the substrate, and its dimensions were 50 mm × 50 mm × 1 mm. Before sputtering, the base pressure in the vacuum chamber was evacuated to 4.655×10^{-4} Pa. The HfB_2 absorber layer was deposited by direct current (DC) magnetron sputtering using a high-purity HfB_2 target (99.99%, diameter = 76.2 mm), while the Al_2O_3 layer was deposited by radio frequency (RF) magnetron sputtering using a high-purity Al_2O_3 target (99.99%, diameter = 76.2 mm). All the coatings were deposited on a substrate with a temperature of 200 °C. The details of the deposition parameters of each layer are listed in Table 1. Furthermore, the same experimental processes and parameters were used to deposit the HfB_2/Al_2O_3 coatings on the Si substrate for measuring the optical constants.

The morphologies of the as-deposited and annealed SS/HfB_2/Al_2O_3 coatings were studied by scanning electron microscopy (SEM, SU8200, Tokyo, Japan). The high-resolution transmission electron microscopy (HR-TEM) image was obtained on Tecnai G2 F20 S-TWIN. X-ray photoelectron spectroscopy (XPS) of Hf, B, O and Al was conducted on ESCALAB 210 (VG Scientific Ltd., UK). Raman spectra were recorded in the range of 150–1000 cm^{-1} using a confocal-micro-Raman technique (LabRAM HR Evolution, HORIBA Jobin Yvon S.A.S., French) at room temperature with an excitation of 532 nm laser light. Spectral reflectance in the wavelength range of 0.3–2.5 μm was measured with a PerkinElmer Lambda 950 UV/vis/NIR spectrometer with an integration sphere (module 150 mm), while the wavelength interval of 2.5–20 μm was obtained on a Bruker TENSOR 27 FT-IR spectrometer equipped with an integrating sphere (A562-G/Q) using a gold plate as a standard for diffuse reflectance. The calculation method of absorptance (α) and emittance (ε) was reported in a previous work.[15]

The coatings were annealed in a resistive tube (Hefei Kejing Materials Technology Co., Ltd, China) to test the thermal

Table 1 Deposition parameters for preparing HfB_2/Al_2O_3 SSAC

Parameters	Value
Substrate	SS and Si
Substrate temperature (°C)	200
Target material	HfB_2 and Al_2O_3
Ar flow rate (sccm)	33
Operating pressure (Pa)	1.03
Sputtering method of HfB_2 layer	DC
Sputtering method of Al_2O_3 layer	RF
HfB_2 target power density (W cm^{-2})	3.29
Al_2O_3 target power density (W cm^{-2})	5.48

stability at the temperature range of 400–700 °C for 2 h with a pressure of 5.0×10^{-1} Pa. Similarly, the long-term thermal stability of the coatings in vacuum and air was investigated for 100 h from room temperature to the desired temperature. The coatings were naturally cooled down in the furnace after annealing.

A spectroscopic phase modulated ellipsometer (HORIBA Jobin Yvon, France) was used to measure the optical constants of the single HfB_2 coatings. The range of the measured optical wavelength was 300–2060 nm, and the incidence angle was 70°. The CODE software was used to simulate the reflectance spectra of the coating.[16]

3. Results and discussion

3.1 Coating structure and spectral selectivity

Fig. 1(a) displays the schematic diagram of SS/HfB_2/Al_2O_3 SSAC. The TEM cross-section image of HfB_2/Al_2O_3 SSAC is shown in Fig. 1(b). The upper Al_2O_3 acted as an anti-reflective layer with a thickness of 59.5 nm, and the bottom HfB_2 acted as an absorber layer with a thickness of 48.5 nm. The HR-TEM images of the HfB_2 and Al_2O_3 layers revealed that each layer was amorphous (Fig. 1(a and d)).

Fig. 1(e) shows the reflectance spectra of the SS substrates, SS/HfB_2 coatings, and SS/HfB_2/Al_2O_3 coatings. The reflectance spectra of SSAC usually show local maxima (R_{max}) and minima (R_{min}) in order to achieve spectral selectivity. The reflectance spectrum of SS/HfB_2 showed R_{min} at $\lambda = 800$ nm, which resulted in a value of $\alpha/\varepsilon = 0.731/0.110$. After depositing the Al_2O_3 layer, two reflectance minima were observed at $\lambda = 502$ nm and $\lambda = 800$ nm, which were caused by the interference effect at the interface between layers.[17,18] The optimized SS/HfB_2/Al_2O_3 coating exhibited a value of $\alpha/\varepsilon = 0.920/0.109$. Clearly, the Al_2O_3 layer greatly improves the solar absorptance and works as the antireflection layer.

The high-resolution XPS spectra with the fitting curves of Hf 4f (7/2, 5/2), B 1s, O 1s, and Al 2p for solar absorber coatings are shown in Fig. 2. The Hf 4f spectrum (Fig. 2(a)) consists of four peaks. The peaks centered at 14.0 eV and 15.4 eV can be assigned to Hf $4f_{7/2}$ and Hf $4f_{5/2}$ of HfB_2, respectively, while the higher intensity peaks at 17.1 eV and 18.8 eV correspond to Hf $4f_{7/2}$ and Hf $4f_{5/2}$ of HfO_2.[19] The B 1s spectrum (Fig. 2(b)) of the single HfB_2 coating consists of two peaks. The peak at 192.1 eV belongs to the B–O bonds of B_2O_3, and the peak at 187.0 eV belongs to the B–Hf bonds of HfB_2. Generally speaking, the B element exhibits stronger affinity for oxygen. The heat of formation for HfO_2 and B_2O_3 was strongly according to the following reaction:

$$HfB_2 + 5/2O_2 \rightarrow HfO_2 + B_2O_3$$
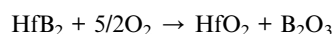
The reaction is favorable at all temperatures with $\nabla G^{o}_{rxn} = -2003 + 0.374$ (kJ).[6]

Fig. 2(c) shows the Al 2p spectrum of the Al_2O_3 coating. A single peak centered at 74.4 eV corresponds to Al_2O_3. Fig. 2(d) shows the O 1s spectrum, where the peaks centered at 531.4 and 532.1 eV are assigned to the characteristics of Al_2O_3, and the
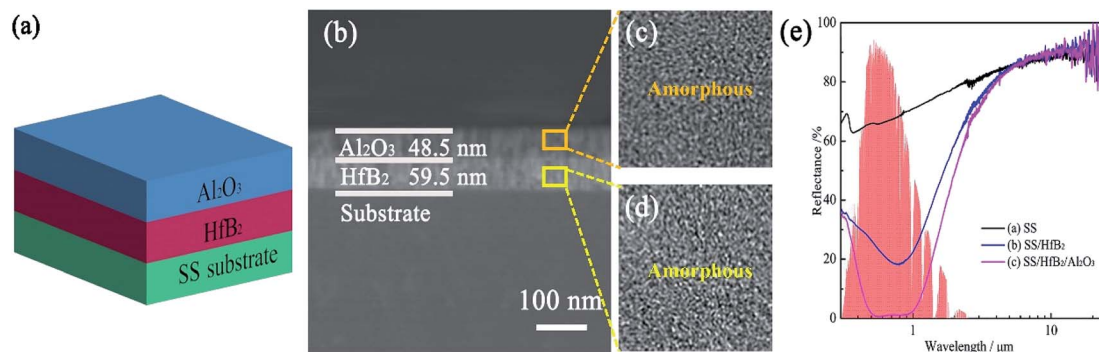
Fig. 1 (a) Schematic diagram of the SS/HfB$_2$/Al$_2$O$_3$ absorber coating. (b) Cross-section image of the HfB$_2$/Al$_2$O$_3$ absorber coating. HR-TEM images of (c) the HfB$_2$ layer and (d) Al$_2$O$_3$ layer. (e) The reflectance spectra of the SS, SS/HfB$_2$ and SS/HfB$_2$/Al$_2$O$_3$ coatings.

peak centered at 530.7 eV belongs to the crystal lattice oxygen (O–Al).[20,21]

3.2 Optical simulation

Generally, the optical constants of films are very different from those of the bulk materials, which strongly depend on the preparation method. Spectroscopic ellipsometry (SE) is an important method for investigating the optical constants of thin films.[22,23] Fig. 3(a) shows the ellipsometric angle (ψ and Δ) spectra measured by SE for the HfB$_2$/Al$_2$O$_3$ coating. The experimental spectra were fitted with a three-layer model. The parameters of the top Al$_2$O$_3$ layer were obtained from the database of the DP2 software. The bottom HfB$_2$ layer was modeled using the Tauc–Lorentz oscillator model because this
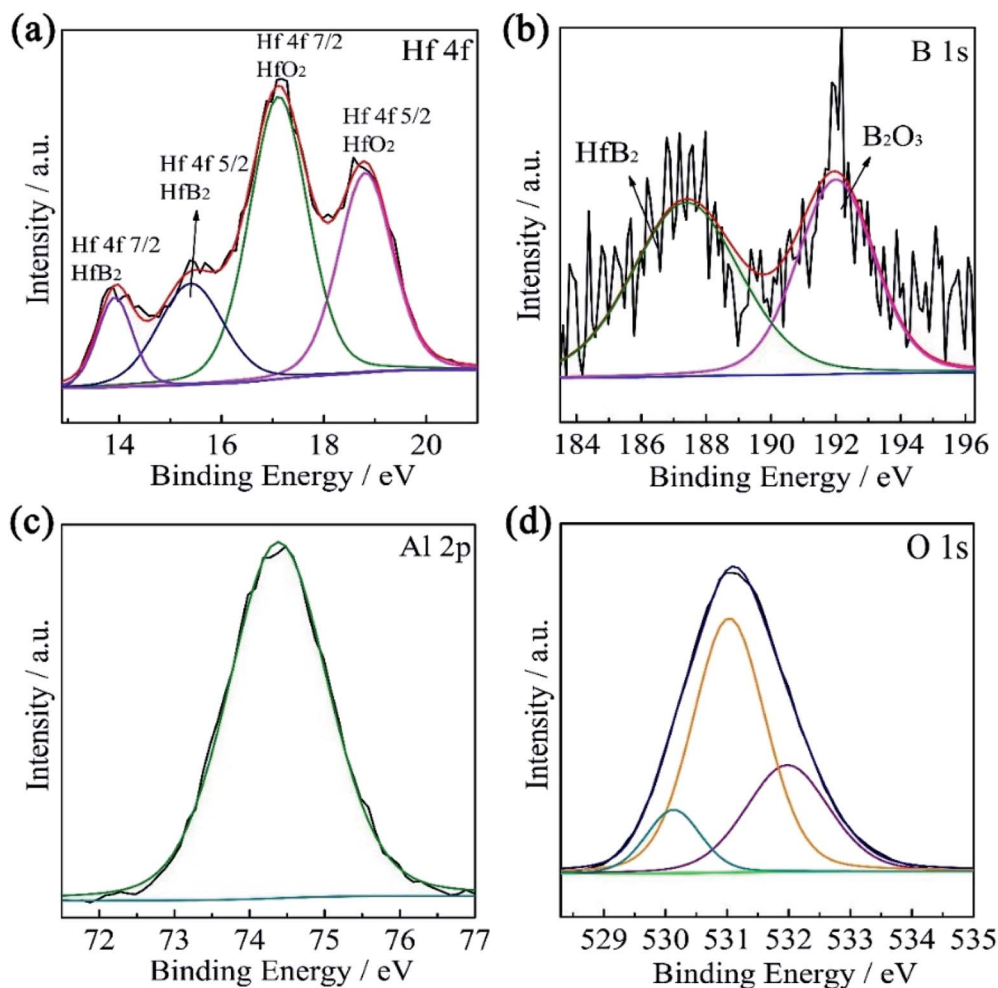

Fig. 2 High-resolution XPS spectra of (a) Hf 4f and (b) B 1s for the single HfB$_2$ layer and (c) Al 2p and (d) O 1s for the top Al$_2$O$_3$ layer.
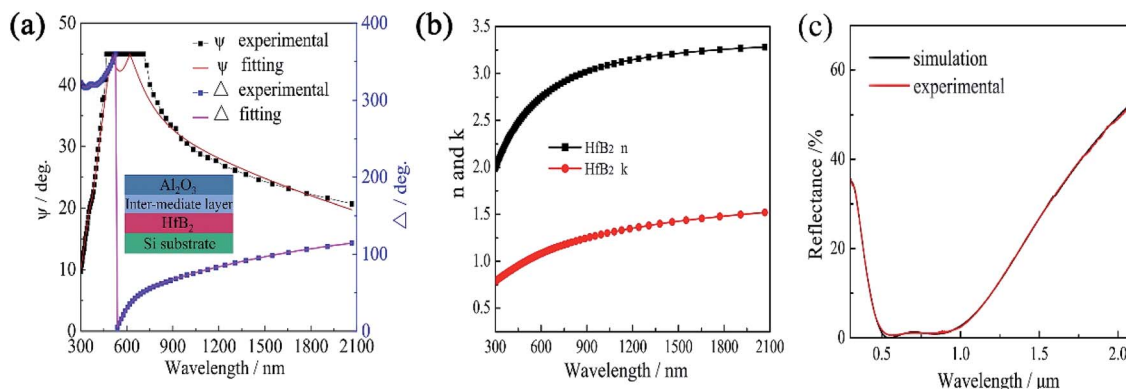
Fig. 3 (a) Experimental and theoretical ellipsometric ψ and Δ spectra for the HfB$_2$/Al$_2$O$_3$ layer deposited on Si substrates. (b) The n and k values for the HfB$_2$ layer and (c) experimental and simulated reflectance spectra of the HfB$_2$/Al$_2$O$_3$ coating deposited on SS substrates.

oscillator model is very effective in the characterization of amorphous materials. In addition, the intermixed layer between HfB$_2$ and Al$_2$O$_3$ was inevitable in the magnetron sputtering process. Hence, an intermediate layer containing 50% HfB$_2$ and 50% Al$_2$O$_3$ was chosen by optimising the composition. The spectra showed great agreement between the experimental value and the theoretical value of (ψ, Δ). The fitting degree of the theoretical value and the experimental value was expressed by χ^2.[24] In this fitting process, $\chi^2 = 2.39$, and the thickness of each layer was HfB$_2$ (59 nm)/intermediate layer (3 nm)/Al$_2$O$_3$ (46 nm).

The formula of the Tauc–Lorentz oscillator model was based on the Tauc expression and the Lorentz oscillator model. The imaginary part of the function is as follows:

$$\varepsilon_2(E) = 2n(E)k(E) = \begin{cases} \dfrac{1}{E} \dfrac{AE_0C(E - E_g)^2}{(E^2 - E_0^2) + C^2E^2} & E > E_g \\ 0 & E < E_g \end{cases} \quad (1)$$

The real part ε_1 was determined from ε_2 with the Kramers–Kronig relation:

$$\varepsilon_1(E) = \varepsilon_\infty + \frac{2}{\pi} P \int_{E_g}^{\infty} \frac{\xi \varepsilon_2(\xi)}{\xi^2 - E^2} \, d\xi \quad (2)$$

Here, P denotes the principal values of the integrals. The fitting parameters are listed in Table 2. The optical constants of the absorption layers were calculated by the DP2 software.

The relationship between the reflectance of the thin film and optical constant is as follows:

$$R = \left| \frac{N_1 - N_2}{N_1 + N_2} \right|^2 = \frac{(n_1 - n_2)^2 + (k_1 - k_2)^2}{(n_1 + n_2)^2 + (k_1 + k_2)^2} \quad (3)$$

Here, $N = n + ik$ is the complex refractive index, which is the most important optical constant of the absorbing medium. The real part n of the equation is the refractive index. The imaginary part k is determined by the attenuation of light waves in the absorbing medium. $K > 0$ indicates that the thermal energy is absorbed by transforming the electromagnetic wave into intrinsic energy. It can be shown from the formula that the reflectance is little when the n and k values of the two media are close. The n value of the HfB$_2$ layer is minimum in the range of 400–800 nm (Fig. 3(b)). In this range, the optical constants of the HfB$_2$ layer and the Al$_2$O$_3$ layer are the closest, which is why there is a presence of local minima in the reflectance spectra of the films.[25]

To simulate the reflectance spectrum of the coating, n, k and thickness of the HfB$_2$ layer and the Al$_2$O$_3$ layer were introduced, and the simulated reflectance spectrum is displayed in Fig. 3(c). In addition, the fitting parameters of the SS substrates were obtained from our previous work.[26] The schematic diagram in the inset of Fig. 3(a) was assumed for simulating the model of the coating. The fit deviation between the simulation and experimental data was 0.00000543, which showed great agreement. This work also confirms that the optical constants obtained from spectroscopic ellipsometry are valid.

3.3 Thermal stability

The SS/HfB$_2$/Al$_2$O$_3$ SSAC materials were annealed in vacuum for 2 h at 400–700 °C to test their thermal stability. Fig. 4 shows the surface micro-morphologies of the as-deposited samples and annealed samples. The surface of the as-deposited coating exhibited a homogeneous structure (Fig. 4(a)). Fig. 4(b–d) show that there is no obvious change in the surface morphologies at a temperature within the range of 400–600 °C. However, when the samples were annealed in vacuum at 700 °C, the size of the grain on the surface increased (Fig. 4(e)). The SEM results indicate that the micro-morphologies of the coating have an excellent thermal stability at 600 °C for 2 h.

Table 2 Optical parameters of HfB$_2$ layer extracted using SE by employing Tauc–Lorentz oscillator model

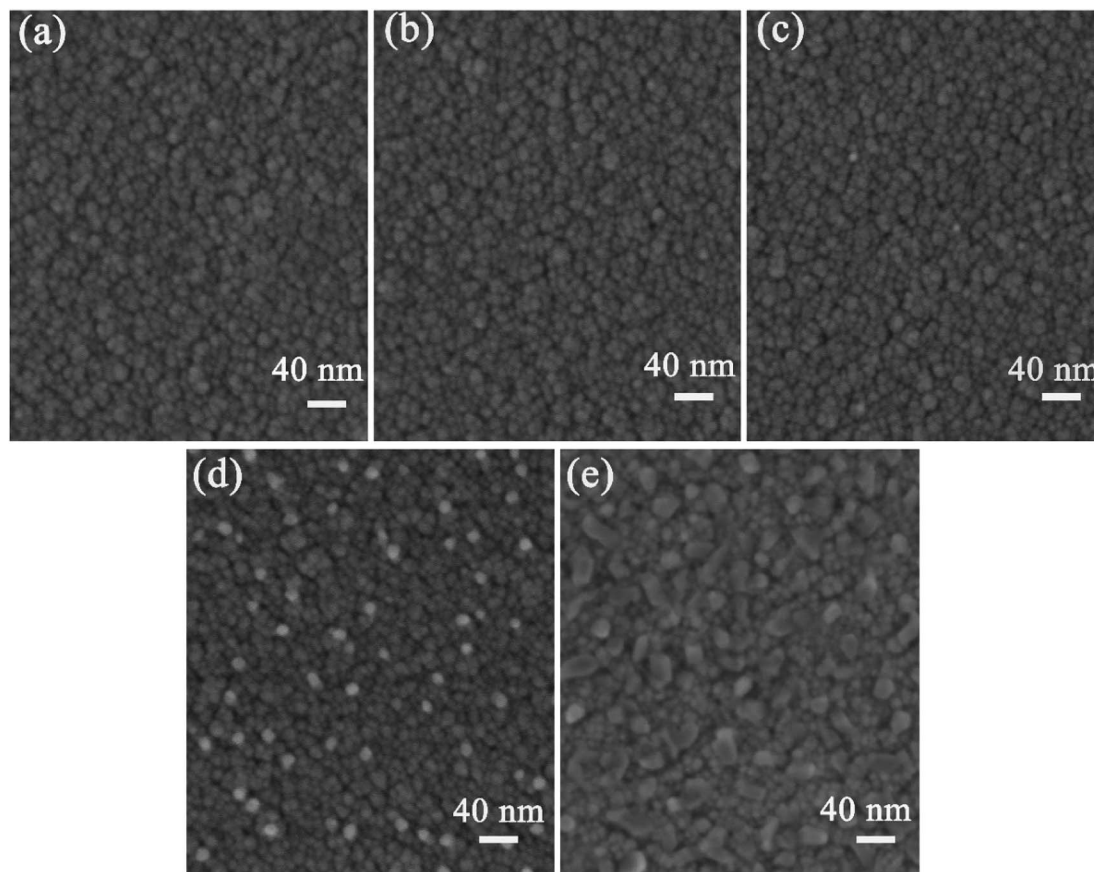| Parameters	Value
The energy band gap E_g	0.101
The peak in the joint density of states E_0	4.526
The high frequency dielectric constant ε_∞	1.479
The optical transition matrix elements A	5.260
Broadening factor C	−3.815

Fig. 4 Surface SEM images of the (a) as-deposited coatings and the coatings annealed at (b) 400 °C, (c) 500 °C, (d) 600 °C and (e) 700 °C for 2 h in vacuum.

The reflectance spectra of the SS/HfB$_2$/Al$_2$O$_3$ coatings, which were annealed in vacuum for 2 h, are shown in Fig. 5(a). The reflectance spectra of the 400–600 °C annealed coatings were similar to that of the as-deposited coating as the wavelength increased, and the values of α and ε did not show any changes ($\Delta\alpha = 0$, $\Delta\varepsilon = 0$). As the temperature increases to 700 °C, the reflectance spectrum shows two local R_{min} values at $\lambda = 410$ nm and $\lambda = 800$ nm as well as a local reflectance maximum (R_{max}) at $\lambda = 670$ nm, which indicate that the coating starts to degrade ($\Delta\alpha = 0.03$, $\Delta\varepsilon = 0$).[27]

Long-term thermal stability of SSAC is another crucial performance index for solar thermal power generation applications. To test this performance, the samples were annealed in vacuum for 100 h at different temperatures (350–600 °C). Fig. 5(b) shows the corresponding reflectance spectra. It is clear that the absorptance of the coatings gradually degrades with the increase in the annealing temperature. When the heat-treatment temperature was higher than 500 °C, the absorptance of the coating dropped below 0.9, and the R_{min} and R_{max} values in the reflectance spectra showed a significant change.

The activation energy (E_g) of the coatings annealed at 350–600 °C for 100 h was calculated by the Arrhenius equation:

$$\ln(\Delta\alpha_s) = \frac{E_g}{RT} + C \qquad (4)$$

Here, $\Delta\alpha_s$ is defined as α(as-deposited) $- \alpha$(post-annealed) at T (units of K) for 100 h, and $R = 8.314$ (universal gas constant). The $\ln(\Delta\alpha_s)$ *versus* 1000/T (K) plots for six temperatures (350–600 °C) were linearly fitted. E_g in this investigation was an indicator that could evaluate the energy that the coating needed to convert from a normal state to an easy degradation state under vacuum. After calculation, E_g of the HfB$_2$/Al$_2$O$_3$ coating was found to be 66.310 kJ mol^{-1}, as shown in Fig. 5(c).

The coatings were also annealed in air for 100 h at different temperatures. Fig. 5(d) displays long-term thermal stability in air by using reflectance spectra at the wavelength of 0.3–25 μm. There was a negligible change in the reflectance spectrum at 400 °C. However, at 500 °C, local R_{max} appeared in the reflectance spectrum at $\lambda = 570$ nm ($\Delta\alpha = -0.019$, $\Delta\varepsilon = -0.026$). When the annealing temperature was increased to 600 °C, a slight redshift of R_{min} was observed from $\lambda = 502$ nm to $\lambda = 616$ nm, and the value of α/ε of the coating was 0.898/0.116. This value indicates that the coating has better thermal stability in air, which is suitable for high-temperature selective solar absorption applications.

3.4 Thermal aging mechanism after air annealing

In order to investigate the failure mechanism of the coating at high temperatures, the microstructure of HfB$_2$/Al$_2$O$_3$ SSAC after
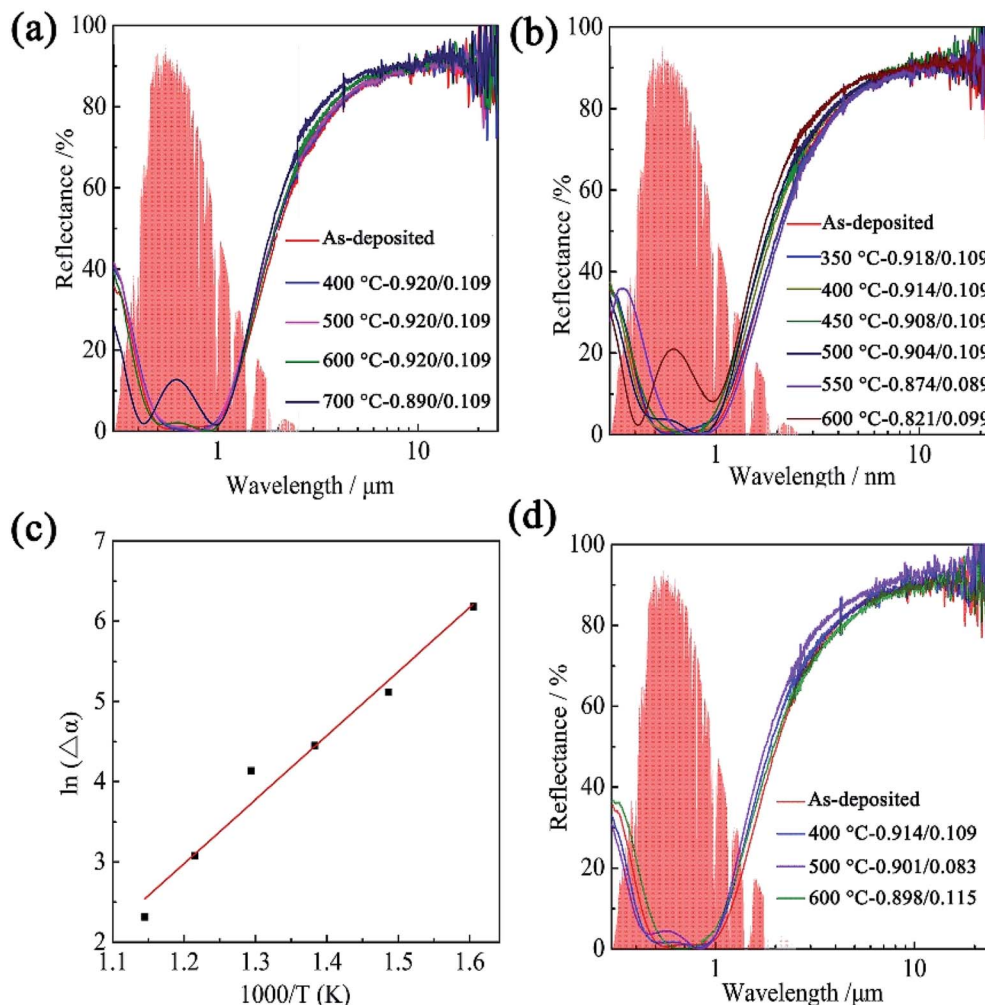
Fig. 5 Reflectance spectra of the annealed coatings for (a) 2 h in vacuum, (b) 100 h in vacuum. (c) Arrhenius plot for the degradation of the coating annealed in vacuum for 100 h. (d) Reflectance spectra of the annealed coatings for 100 h in air.

annealing was analyzed using micro-Raman spectrometry. The Raman spectra of the coatings annealed at 600 °C in air are shown in Fig. 6. The bands centered at 100–175 cm^{-1} and

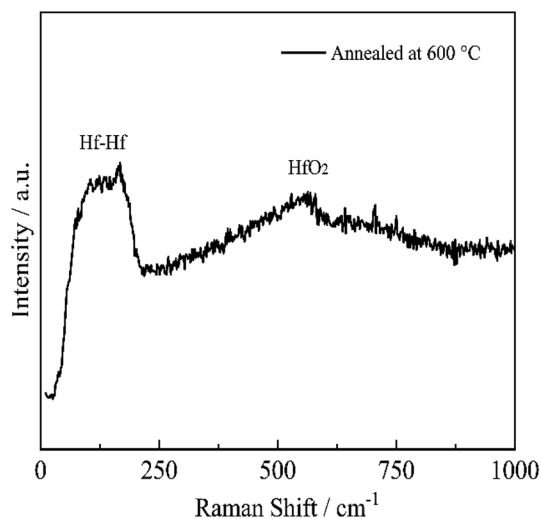Fig. 6 The Raman spectra of the coating annealed at 600 °C in air.

552 cm^{-1} are observed, which originate from the vibrations of HfO$_2$.[28] The atomic (Hf, O) contribution for each normal mode for HfO$_2$ is listed in Table 3. Considering the Raman spectrum, we can confirm that the formation of HfO$_2$ leads to the degradation of optical properties.

Ellipsometry was also used to investigate HfB$_2$/Al$_2$O$_3$ SSAC after annealing at 600 °C in air, which was deposited on the Si substrate by magnetron sputtering. The detailed experimental

Table 3 Raman frequencies and the atomic (Hf, O) contribution for each normal mode

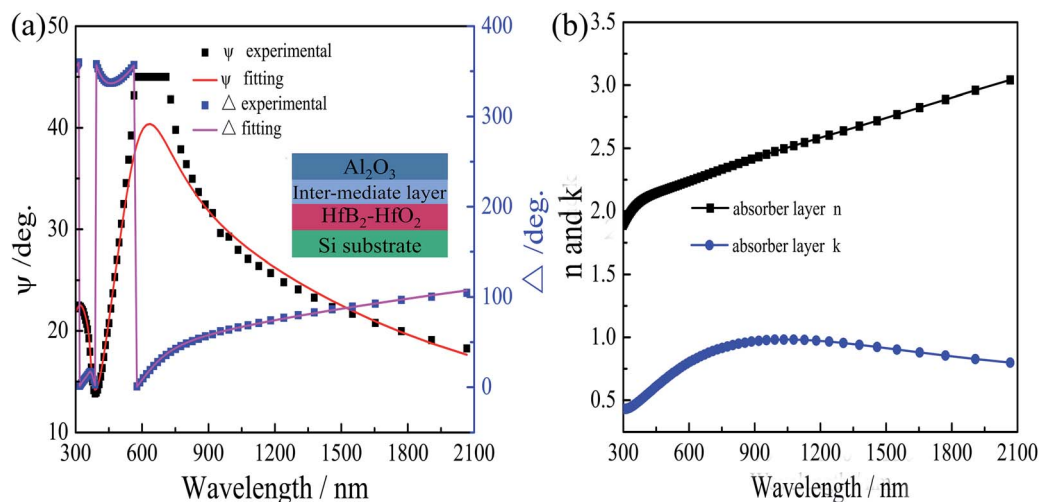| Raman frequency[28] (cm^{-1})	Hf (%)	O (%)	Experimental values of this work (cm^{-1})
113	30	70	100–175
133	95	5	
133	74	26	
149	99	1	
164	99	1	
551	2	98	552

Fig. 7 (a) Experimental and theoretical ellipsometric ψ and Δ spectra for the 600 °C annealed coating. (b) The n and k values for the absorber for the 600 °C annealed coating.

Table 4 The optical constants (n and k at 550 nm) of the HfB$_2$ layers

Layer	As-deposited coating		Annealed at 600 °C in air	
	n	k	n	k
Absorber layer	2.68	1.04	2.19	0.73

parameters of the involved layer were the same as those of the single layer, as mentioned above, and the ellipsometric spectra are shown in Fig. 7. Based on the Raman spectra of the 600 °C-annealed coating, a three-layer model was established, which is shown in the inset of Fig. 7(a). The dispersion model of the HfB$_2$–HfO$_2$ layer was modeled with the Tauc–Lorentz dispersion formula, and the doped layer contained 70% HfO$_2$ and 30% HfB$_2$. The Lorentz oscillators were used to describe the optical functions of the Al$_2$O$_3$ layers. The experimental ellipsometric angle ψ and Δ of the tandem absorber coating were best fitted with the theoretical spectra, as shown in Fig. 7(a). In this fitting process, χ^2 was 2.3. The thicknesses of the HfB$_2$–HfO$_2$ layer, intermediate layer, and Al$_2$O$_3$ layer were 59 nm, 3 nm, and 46 nm, respectively. The n and k values of the absorber layer obtained from the ellipsometric spectra of the annealed coating are shown in Fig. 7(b). Table 4 shows the optical constants of the absorber layers at a reference wavelength of 550 nm. The n and k values of the absorber layer were lower than those of the pristine absorber coating. This result indicated that the composition of the coatings changed after annealing at 600 °C in air, which was caused by the oxidation of HfB$_2$.

4. Conclusions

A novel SS/HfB$_2$/Al$_2$O$_3$ tandem absorber was prepared, which exhibited high solar spectrum selectivity (α/ε) of 0.920/0.109. The high optical constants of the HfB$_2$ layers measured from

SE clearly revealed that the HfB$_2$ layer was the main absorber layer. The CODE optical simulation program was used to simulate the reflectance spectra of SS/HfB$_2$/Al$_2$O$_3$ SSAC, and the deviation between the simulation and experimental data was 0.00000543. The thermal stability test indicated that the HfB$_2$/Al$_2$O$_3$ absorber coating was thermally stable in vacuum at 600 °C for 2 h. After extending the annealing time to 100 h, the coating could maintain high spectral selectivity after aging at 500 °C irrespective of whether in air or vacuum. The thermal stability test in vacuum for 100 h also indicated that the activation energy of the SS/HfB$_2$/Al$_2$O$_3$ coating was about 66.31 kJ mol^{-1}.

Conflicts of interest

There are no conflicts to declare.

Acknowledgements

References

1 F. Cao, K. McEnaney, G. Chen and Z. Ren, *Energy Environ. Sci.*, 2014, **7**, 1615–1627.
2 S. K. Sansaniwal, V. Sharma and J. Mathur, *Renewable Sustainable Energy Rev.*, 2018, **82**, 1576–1601.
3 N. Selvakumar and H. C. Barshilia, *Sol. Energy Mater. Sol. Cells*, 2012, **98**, 1–23.
4 X.-H. Gao, Z.-M. Guo, Q.-F. Geng, P.-J. Ma, A.-Q. Wang and G. Liu, *Sol. Energy Mater. Sol. Cells*, 2017, **163**, 91–97.

5 K. Hans, S. Latha, P. Bera and H. C. Barshilia, *Sol. Energy Mater. Sol. Cells*, 2018, **185**, 1–7.

6 W. G. Fahrenholtz, G. E. Hilmas, I. G. Talmy and J. A. Zaykoski, *J. Am. Ceram. Soc.*, 2007, **90**, 1347–1364.

7 J. Zou, S. Grasso, L.-F. Liu, H.-B. Ma, M. Reece and J. Binner, *Scr. Mater.*, 2018, **156**, 115–119.

8 E. Sani, L. Mercatelli, J.-L. Sans, L. Silvestroni and D. Sciti, *Opt. Mater.*, 2013, **36**, 163–168.

9 C. Musa, R. Licheri, R. Orrù, G. Cao, A. Balbo, F. Zanotto, L. Mercatelli and E. Sani, *Sol. Energy*, 2018, **169**, 111–119.

10 N. Selvakumar, N. T. Manikandanath, A. Biswas and H. C. Barshilia, *Sol. Energy Mater. Sol. Cells*, 2012, **102**, 86–92.

11 D. Sciti, L. Silvestroni, L. Mercatelli, J.-L. Sans and E. Sani, *Sol. Energy Mater. Sol. Cells*, 2013, **109**, 8–16.

12 E. Sani, L. Mercatelli, D. Jafrancesco, J. L. Sans and D. Sciti, *J. Eur. Opt. Soc. Rapid Publ.*, 2012, **7**, 12052.

13 E. Sani, M. Meucci, L. Mercatelli, D. Jafrancesco, J.-L. Sans, L. Silvestroni and D. Sciti, *J. Photonics Energy*, 2014, **4**, 045599.

14 E. Sani, L. Mercatelli, M. Meucci, L. Silvestroni, A. Balbo and D. Sciti, *Sol. Energy Mater. Sol. Cells*, 2016, **155**, 368–377.

15 X.-H. Gao, Z.-M. Guo, Q.-F. Geng, P.-J. Ma, A.-Q. Wang and G. Liu, *RSC Adv.*, 2016, **6**, 63867–63873.

16 M. Theiss, *Hard and Software for Optical Spectroscopy*, Dr Bernhard-Klein-Str. 110 52078 Aachen, Germany, 2013.

17 J. Jyothi, H. Chaliyawala, G. Srinivas, H. S. Nagaraja and H. C. Barshilia, *Sol. Energy Mater. Sol. Cells*, 2015, **140**, 209–216.

18 W. Wang, H. Wen, S. Ling, Z. Li, J. Su and C. Wang, *J. Mater. Chem. A*, 2018, **6**, 15690–15700.

19 C. Monticelli, A. Bellosi, F. Zucchi and M. Dal Colle, *Electrochim. Acta*, 2007, **52**, 6943–6955.

20 T. Schroeder, G. Lupina, O. Seifarth, M. Tallarida and D. Schmeißer, *J. Appl. Phys.*, 2007, **102**, 014103.

21 X.-H. Gao, Z.-M. Guo, Q.-F. Geng, P.-J. Ma, A.-Q. Wang and G. Liu, *Sol. Energy Mater. Sol. Cells*, 2017, **164**, 63–69.

22 T. W. H. Oates, H. Wormeester and H. Arwin, *Prog. Surf. Sci.*, 2011, **86**, 328–376.

23 M. Rasheed and R. Barillé, *J. Non-Cryst. Solids*, 2017, **476**, 1–14.

24 A. Dana, H. C. Barshiliab, K. Chattopadhyay and B. Basu, *Renewable Sustainable Energy Rev.*, 2017, **79**, 1050–1077.

25 X.-H. Gao, W. Theiss, Y.-Q. Shen, P.-J. Ma and G. Liu, *Sol. Energy Mater. Sol. Cells*, 2017, **167**, 150–156.

26 X.-H. Gao, C.-B. Wang, Z.-M. Guo, Q.-F. Geng, W. Theiss and G. Liu, *Opt. Mater.*, 2016, **58**, 219–225.

27 S. Zhao and E. Wackelgard, *Sol. Energy Mater. Sol. Cells*, 2006, **90**, 243–261.

28 C. W. Li, M. M. McKerns and B. Fultz, *Phys. Rev. B*, 2009, **80**, 054304.